Analytical Behaviour of Rectangular Concrete Filled Stainless Steel Tubular Columns under Bi-axial Eccentric Compression

IOP Conf. Series: Materials Science and Engineering **490** (2019) 032004 doi:10.1088/1757-899X/490/3/032004

Analytical Behaviour of Rectangular Concrete Filled Stainless Steel Tubular Columns under Bi-axial Eccentric Compression

Yongjin Li [1,*], Wenhua Liu[1] and Hao Han[1]

[1]College of Transportation and Civil Engineering, Fujian Agriculture and Forestry University, Fuzhou, Fujian, 350002, China

*Corresponding author e-mail: liyongjin@tsinghua.edu.cn

Abstract. The aim of this paper is to numerically investigate the behavior of the rectangular concrete filled stainless steel tubular (CFSST) columns subjected to bi-axial eccentric compression. A finite element (FE) model for modelling the bi-axial eccentric compressive behaviour was established. The FE predictions were verified against the test results. Behaviour analysis was then performed to investigate the typical curves of load versus deformation, the internal force distribution, stress development and interaction of stainless steel tube and core concrete during the loading process.

1. Introduction

In recent years, the mechanism of concrete filled stainless steel tube (CFSST) structures has been studied by some researchers. The topics included the static behaviour under the axial compression [1-6] and the uni-axial eccentric compression [2]; the cyclic behaviour [7]; the behaviour of CFSST X-joints subjected to compression [8]; and the fire behaviour [9]. However, the work on the behaviour of CFSST columns under bi-axial eccentric compressive loading was not been reported in the past literatures.

To fill the research gap, this paper thus presents a investigation of the mechanical behaviour of the rectangular CFSST bi-axial eccentric compression columns by establishing the rational finite element (FE) analysis model.

2. General description

A FE model, based on the contribution of Tao et al. [6], for the simulation of rectangular CFSST bi-axial eccentric compression columns is developed. The model considers core concrete and steel tube as C3D8R elements and S4 elements, respectively. The FE mesh with appropriate mesh density for a typical CFSST column is given in Fig. 1 for CFSST with rectangular sections.

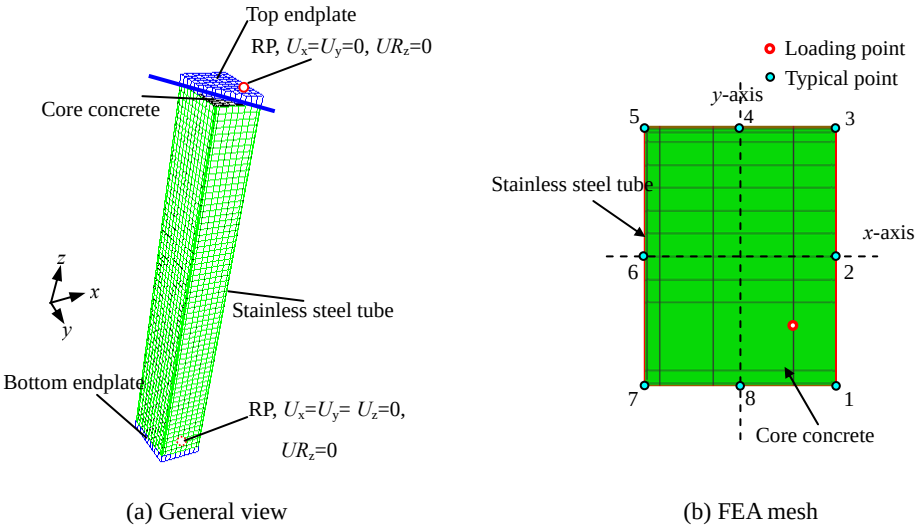

(a) General view (b) FEA mesh

Figure 1. Typical finite element model

The material and contact models were presented in Tao et al. [6]. The boundary conditions were also shown in Fig. 1. Pin-ended conditions were used in the FE model, and the point in the loading plate, which deviated from the center of the column section with the load eccentricity e_x and e_y in the x-axis and y-axis directions, was taken as the loading point. The loading plate was assumed to be a rigid block with stiffness large enough so that deformation could be neglected, and the load eccentricities of the bottom and top loading plates were the same. All degrees of freedom except rotation around the x-axis and y-axis on the loading point were constrained for the bottom loading plate. Displacements in the x-axis and y-axis directions and rotation around the z-axis on the loading point were constrained for top loading plate. An axial compression load was applied at an appointed displacement on the loading point of the top loading plate along the z-axis.

Additionally, the initial geometric imperfections and enhanced strength corner properties of steel tube were also considered in above FE model. More details can be found in Tao et al. [6].

3. Verifications of the FE model

For verifying the mentioned FE model, a comparison from the tested results (Li et al. [10]) and FE results is conducted. The failure mode using FE model is compared with the measured one in Fig. 2. The simulated typical N (load) versus u_m (mid-height lateral deflection) curves are given in Fig. 3. Comparisons of the predicted peak strengths (N_{uc}) and tested ultimate strength (N_{ue}) are shown in Fig. 4. A mean ratio (N_{uc}/N_{ue}) of 1.007 is gained with a standard deviation of 0.018.

Form above comparisons, it can be deduced that this proposed FE model can simulate the behaviour of bi-axial eccentric compressive CFSST column with reasonable accuracy and can be used to carry out the further mechanism analysis.

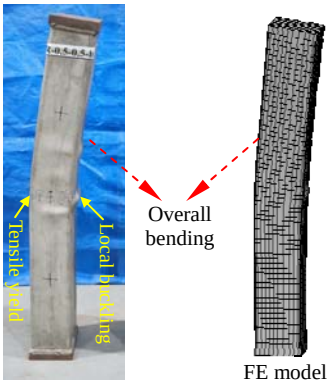

Figure 2. Failure mode of typical specimen (r-0.5-0.5-b)

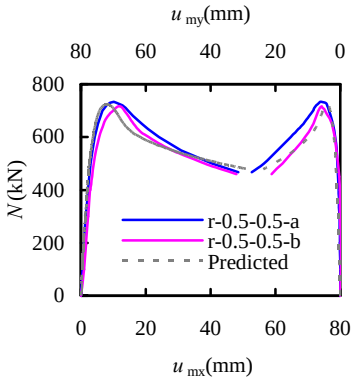

Figure 3. Comparisons of predicted and measured N-u_m relations (r-0.5-0.5)

4. Analysis and discussions

4.1. Load versus deformation relation

Taking the parameter of specimen r-0.5-0.5 presented in Li et al. [10] as an example, the behaviour of typical rectangular CFSST member under bi-axial eccentric compression was investigated by FE model.

For convenience of analysis, the resultant displacement (u_m) is adopted to replace the mid-height lateral deflection components u_{mx} and u_{my}. It can be expressed as:

$$u_m = \sqrt{u_{mx}^2 + u_{my}^2} \tag{1}$$

The graph of typical N-u_m relation for rectangular bi-axial eccentric compression CFSST member is given in Fig. 5, where the loads of the core concrete and stainless steel tube are also shown. In this curvature, 4 feature points are marked, i.e., the stainless steel compressive yield point (point A), the tension stainless steel tube yield point (point B), the peak value point (point C) and the failure point (point D, where the load drops to $0.85N_u$). The four stages in the graph are analyzed as follows:

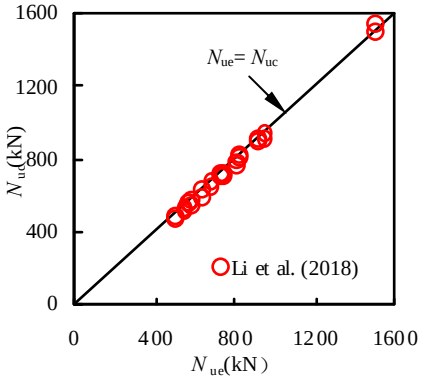

Figure 4. Comparisons between predicted and experimental ultimate strength

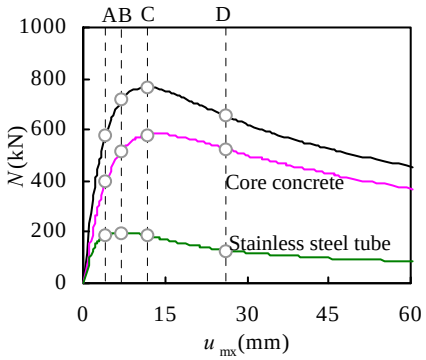

Figure 5. Typical N-u_m relations of rectangular CFSST member

Stage I (OA) is the elastic stage. According to concrete and stainless steel tube stiffness, the load is

carried and shared by them. Stage II (AB) is the elastic-plastic stage. The column rigidity tends to drop gradually, and the large part of load is carried by core concrete whereas the load of stainless steel tube slightly increases. Stage III (BC) is the plastic stage. For core concrete, the load continuously increases until the member strength reaches the peak value, whereas the load of stainless steel tube starts to decrease. Additionally, the rigidity of the member is lower than that of the Stage II. Stage IV (CD) is the descending stage. The load of core concrete starts to decrease with increase in the overall bending of the CFSST.

4.2. Stress distribution

The core concrete stress distributions of the mid-height section at different feature points are given in Fig. 6, where the compressive stress is unified by the cylindrical compressive strength (f_c'=59.2MPa) and the tensile stress is expressed in terms of the concrete tension strength (f_t=4.6MPa).

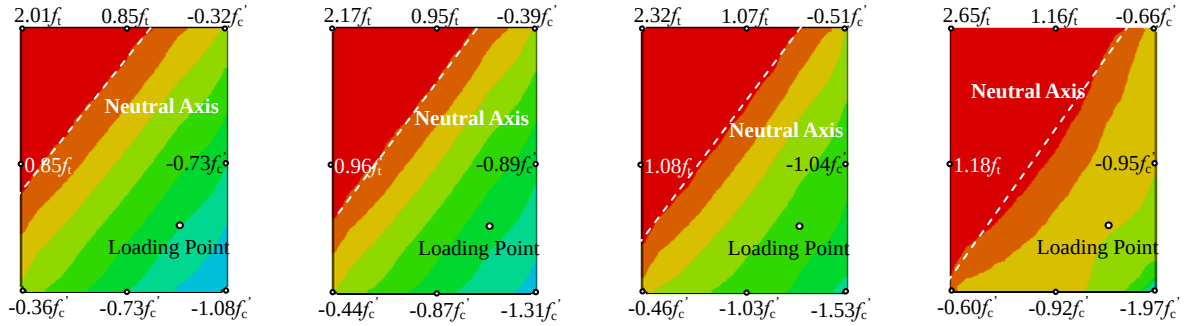

(a) Point A (b) Point B (c) Point C (d) Point D

Figure 6. Concrete stress distributions at the mid-height section

It can be seen from Fig. 6 that, corresponding to the same bi-axial eccentricity ratio (e_x/r_x = e_y/r_y =0.5, and e_x/e_y = B/D in this case), the sections are divided into compressive and tensile zones by neutral axis where stress is zero, and the neutral axes are inclined at an angle θ = arctan (D/B) to the x-axis direction before point C. The concrete stresses of both compressive and tensile zones develop during the loading, and the neutral axis moves increasingly towards the compression side which indicates that the sectional tension zone increases gradually. Additionally, except for the corner regions, the stress value of concrete is approximately proportional to the distance away from neutral axis until the ultimate capacity is reached. Therefore, the maximum compressive stress and tensile stress occur at the concrete corner near point 1 and point 5 (as shown in Fig. 1(b)), respectively.

As the enhanced strength corner properties result in improved confinement, the maximum longitudinal compressive and tensile concrete stress exceeds f_c' and f_t, from the compressive stainless steel yields (point A in Fig. 5), respectively. The concrete stress at these corner regions continuously increases even when the member is beyond the capacity. For the flat regions, the concrete stress raises until the member strength reaches the peak, and the stress value of midpoint of the flat region also exceeds f_c' and f_t due to the confinement effect. After the peak load, the core concrete stress level of the compressive zone starts to reduce.

Fig. 7 depicts the Mises stress (σ_{mises}) versus deflection (u_m) relations for stainless steel tube at different positions. It shows that the stainless steel gradually yields as the distance from the neutral

axis of the section decreases. Firstly, the extreme compression fiber of stainless steel tube (Point 1 in Fig. 1(b)) yields. After that, the midpoints of flag region, at the compressive side of the section near the loading point, reach their yield stress. Then the extreme tensile fiber on the mid-height section (Point 5 in Fig. 1(b)) attains the yield strength. However, for other characteristic points in Fig. 1(b), the stainless steel does not yield before the peak load.

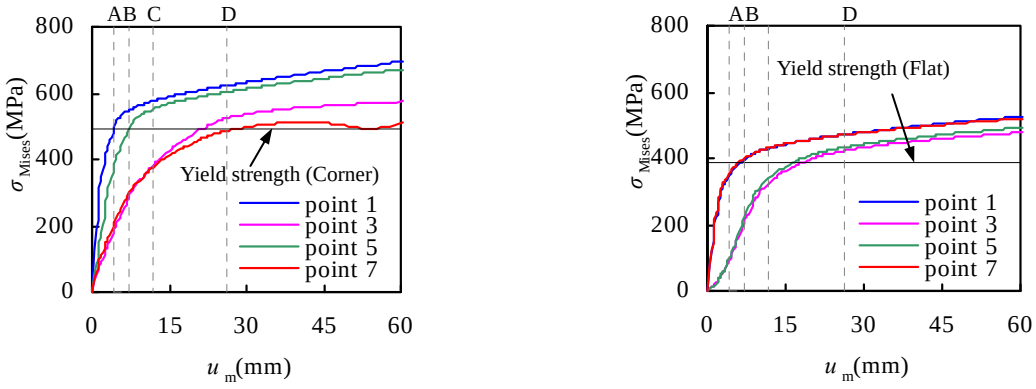

(a) Midpoint of the corner arc (b) Midpoint of the flat region

Figure 7. Stress (σ) versus deflection (u_m) curves of stainless steel

4.3. Interaction between stainless steel tube and core concrete

To illustrate the confinement of the stainless steel tube to the core concrete, eight different points (shown in Fig. 1 (b)) are selected to investigate the interaction stress (p) between the stainless steel tube and core concrete. The p-u_m curves are given in Fig. 8. The values of p near the corner regions (Fig. 8 (a)) are much higher than those at the midpoints of the flat regions (Fig. 8 (b)), which indicates that the corners regions of rectangular stainless steel tube can provide much stronger confinement. It also can be found from Fig. 8 (a) that, the longer the distance between the point and neutral axis, the values of p are higher and develop faster.

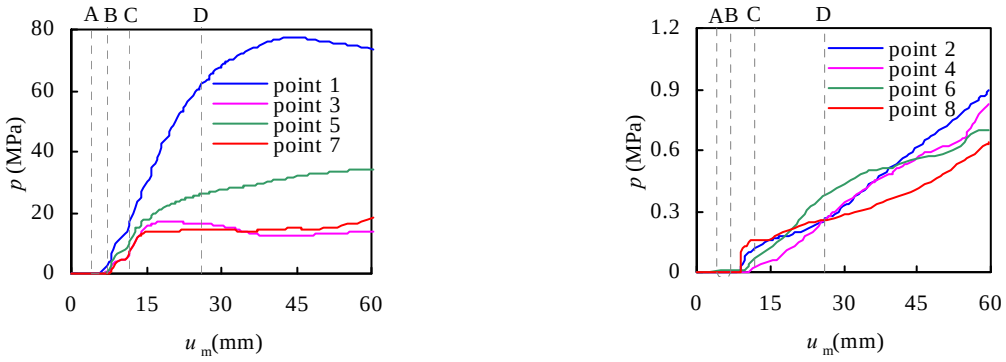

(a) Midpoint of the corner arc (b) Midpoint of the flat region

Figure 8. Contract stress (p) versus deflection (u_m) relations

5. Conclusions

Based on this study, the following conclusions can be drawn:

1) The FE model presented in this paper could show a acceptable simulation of the failure mode and the N-u_m curves.

2) The FE analysis showed that the stress levels of both stainless steel and core concrete, as well as the interaction between stainless steel and core concrete were related to their location to the neutral axes of the cross-section, even through the strength enhancement at the corner regions of stainless steel.

3) The stress of core concrete exceeded the compressive strength of the concrete cylinder due to the confinement action of the stainless steel tube to the core concrete.

Acknowledgements

The study of this paper is supported by the National Natural Science Foundation of China (51308121), the Provincial Natural Science Foundation of Fujian (2018J01632) and the China Scholarship Council (CSC). These financial supports are highly appreciated.

References

[1] Young B, Ellobody E. Experimental investigation of concrete-filled cold-formed high strength stainless steel tube columns. J Constr Steel Res. 62(2006), 5, p. 484-492.

[2] Uy B, Tao Z, Han LH. Behaviour of short and slender concrete-filled stainless steel tubular columns. J Constr Steel Res. 67(2011) , 3, p. 360-378.

[3] Dabaon MA, El-Boghdadi MH, Hassanein MF. Experimental investigation on concrete-filled stainless steel stiffened tubular stub columns. Eng Struct. 31(2009) , 2, p. 300-307.

[4] Chang X, Ru ZL, Zhou W, Zhang YB. Study on concrete-filled stainless steel–carbon steel tubular (CFSCT) stub columns under compression. Thin-Walled Struct. 63(2013) , 3, p. 125-133.

[5] Ellobody E, Ben Y. Design and behaviour of concrete-filled cold-formed stainless steel tube columns. Eng Struct. 28(2006) , 4, p. 716-728.

[6] Tao Z, Uy B, Liao FY, Han LH. Nonlinear analysis of concrete-filled square stainless steel stub columns under axial compression. J Constr Steel Res. 67(2011) , 11, p. 1719-1732.

[7] Liao FY, Han LH, Tao Z, Rasmussen KJR. Experimental behavior of concrete-filled stainless steel tubular columns under cyclic lateral loading. Journal of Structural Engineering ASCE. 143(2017), 4, p.1-15.

[8] Feng R, Young B. Behaviour of concrete-filled stainless steel tubular X-joints subjected to compression. Thin-Walled Struct. 47(2009) , 4 , p. 365-374.

[9] Han LH, Chen F, Liao FY, Tao Z, Uy B. Performance of concrete filled stainless steel tubular columns in fire. Eng Struct. 56(2013) , 11, p. 165-181.

[10] Li YJ, Liao FY, Huang HQ. Experimental study on behaviour of concrete filled rectangular stainless steel tubular columns under bi-axial eccentric compression. Progress in Steel Building Structures. 20(2018) , 2, p. 60-66 [in Chinese].